NASA TECHNICAL MEMORANDUM

NASA TM- 75775

UNSTEADY EFFECTS OF A CONTROL SURFACE IN TWO-DIMENSIONAL SUBSONIC AND TRANSONIC FLOW

R. Grenon, A. Desopper and J. Sides

Translation of "Effets instationnaires d'une gouverne en écoulement bidemensionnel subsonique et transsonique", AGARD Conference Proceedings No. 262, Advisory Group for Aerospace Research and Development, NATO, September 1979, pp. 19-1 to 19-14. (Report AGARD-CP-262)

NATIONAL AERONAUTICS AND SPACE ADMINISTRATION
WASHINGTON, D.C. 20546 JUNE 1980

Notation

a : speed of sound

ρ : voluminal mass

V : speed of flow

M : Mach number

c : chord

α : incidence of airfoil

δ : angle of flap, positive downwards

δ_m : average angle of flap

δ_i : amplitude of oscillations of flap

t : time

ω : circular frequency

$f = \frac{\omega}{2\pi}$: frequency of oscillations (Hz)

$k = \frac{\omega c}{2 V_\infty} = \frac{\pi f c}{V_\infty}$: reduced frequency

P : instantaneous pressure

P_m : average pressure

ΔP : fluctuation of pressure

$K_p = \frac{P - P_\infty}{\frac{1}{2}\rho_\infty V_\infty^2}$: coefficient of instantaneous (or steady) pressure

$C_p = \frac{\Delta P}{\frac{1}{2}\rho_\infty V_\infty^2 \delta_i}$: coefficient of unsteady pressure

K_p^* : value of K_p when $M_\ell = 1$

C_z : steady lift coefficient

C_{z_δ} : unsteady lift coefficient

C_{m_δ} : coefficient of steady of moment pitch

C_{mc_δ} : coefficient of unsteady moment of hinge

φ : angle of phase

P_i : generating pressure

Re : Reynolds number

Coefficients

m : average values (δ . P)

ℓ : local values (a , V , M)

∞ : values to infinity upstream (a , V , M)

1 : indicator assigned to the module and phase of first harmonic of C_p .

UNSTEADY EFFECTS OF A CONTROL SURFACE IN TWO-DIMENSIONAL SUBSONIC AND TRANSONIC FLOW

R. Grenon, A. Desopper and J. Sides
Office national d'Etudes et de Recherches Aérospatiales
(ONERA) 92320 Chatillion (France)

1. Introduction

The design of present-day aircraft is more and more governed by /19-2* the use of Control Configured Vehicle (CCV) techniques which require utilization of control surfaces with a short response time. With this in view, ONERA undertook an in-depth study of the unsteady effects of an oscillating control surface.

This presentation more specifically concerns results obtained in subsonic and transonic two-dimensional flow on an airfoil equipped with a trailing edge control surface involving 25% of the chord, to which a sinusoidal motion can be imparted.

We first briefly recall the principal experimental results of steady and unsteady pressure measurements carried out on this airfoil in the S3 wind tunnel at Modane. These results have already been the subject of a presentation at an AGARD meeting in 1977 (1).

Then we compare these experimental results with those obtained using various methods for calculating steady and unsteady inviscid flows. Finally, we present the results of the first attempts to take into account the effects of viscosity in unsteady flow.

2. Summary of Principal Experimental Results

2.1 Presentation of Test Material

For this study, carried out in close collaboration by the

*Numbers in margin indicate pagination in the foreign text.

Aeordynamics and Structural Resistance departments of ONERA, the selected airfoil is a supercritical airfoil of 16% relative thickness, developed by the Aérospatiale company (airfoil RA 16 SC 1).

The two-dimensional model has a chord of 180 mm. The control surface of the trailing edge, involving 25% of the chord, is activated by two small rotary hydraulic actuators controlled by synchronized servo-valves and driven by a sinusoidal signal generator. This system makes it possible to obtain oscillations of the control surface of $\pm 1^{\circ}$ at 100 Hz, the amplitude reaching $\pm 5^{\circ}$ at 20 Hz (figure 1).

The model is equipped with 78 static pressure gauges and 32 Kulite short response time unsteady pressure gauges.

The test took place in the S3 "gust" wind tunnel at Modane, at Mach numbers between 0.3 and 0.8. The test program comprises a steady and an unsteady segment, with study of the influence of numerous parameters. The treatment of the signal collected by the Kulite gauges during the dynamic test is detailed in Figure 2.

Finally, a strioscopy bench made it possible to film the movement of the extrados shock wave in transonic mode.

2.2 Steady Characteristics of the Airfoil

At zero incidence and zero flap angle, a supersonic zone appears at the extrados trailing edge in the vicinity of $M_{\infty} = 0.7$ (Figure 3). As the Mach number increases, this supersonic zone rapidly extends downstream, giving a distribution of pressure in the form of a plateau with a rather weak shock, and the intrados in its turn becomes supersonic.

The appearance of the supersonic zones is profoundly altered by the angling of the flap (Figure 4), but, as the airfoil is heavily /19-4 loaded towards the rear because of its design (Figure 3), the control surface remains positively loaded in most cases, the load on the control

surface being cancelled only for a flap angle in the neighborhood of $\delta = -10^{\circ}$.

2.3 Unsteady Characteristics of the Airfoil

The various coefficients of unsteady pressure, lift, moment of pitch and moment of hinge are presented in the form of the modulus and phase of the first harmonic (ω term of the Fourier series). This mode of presentation is justified by the experiment, the harmonics of the higher order being negligible except very locally for pressure signals in the narrow zones swept by the shocks. The phases are determined in relation to the position of the control surface and the extrados pressure phases are presented with an interval of 180°; this would make it possible to obtain the same phase curve for the intrados and extrados in the case of a symmetrical airfoil at zero incidence with a control surface oscillating around a zero flap angle; here this will demonstrate the effect of the dissymetry of the airfoil which was used.

Influence of the Mach Number

First we note the importance of the influence of the Mach number on the distribution of the unsteady pressure coefficients for the same reduced frequency (Figure 5). In subcritical regime the curve of the Cp 1 moduli shows the classic appearance anticipated in the plane plate theory (maxima at the leading edge and at the hinge corresponding to the infinite values of the theory), the phase evolving in almost linear fashion from a lag at the leading edge to a lead at the flap.

As the Mach number increases, a supersonic zone forms, terminating in a shock of variable intensity. The oscillations of this shock are reflected on the curve of the moduli by a peak whose intensity depends on that of the shock. The level of pressure fluctuations upstream from the shock, that is, in the supersonic flow zone, diminishes as the Mach number increases.

The difference in phase increases with the Mach number at the leading edge, but it maintains an almost steady level in the supersonic

zone and shows an abrupt leap at the level of the shock.

The appearance of the unsteady pressure distributions is thus very different depending on whether we are in subcritical regime, without shocks, or in supercritical regime, with shocks.

Influence of the Reduced Frequency

The influence of the reduced frequency, moreover, is reflected somewhat differently in the two cases. In subcritical regime, the modulus of pressure diminishes and the phase lag at the leading edge grows as the reduced frequency increases, the zero phase joint being displaced upstream (Figure 6). In supercritical regime, while the phase lag in the supersonic zone increases with the reduced frequency, the unsteady pressure moduli, in contrast, evolve in the opposite direction on either side of the shock (Figure 7).

Steady-Unsteady Interactions

Contrary to the results anticipated by the linear theory, /19-4
there is significant interaction of the average characteristics of the flow on its unsteady characteristics. This interaction is well illustrated by the effect of average angle of the flap on the unsteady pressures (Figures 8 and 9). When the average angle of the flap increases, thus increasing the average load on the wing and on the control surface, the moduli of the unsteady pressures diminish, and the phases evolve slightly in the direction of a phase lead. However, a strong increase in unsteady pressures at the trailing edge appears when the flap oscillates increasingly near breakaway ($\delta m = 2.5$ in the present case). In supercritical regime (Figure 9) to an increasing degree, we observe translation of the peak of the curve of moduli and of the jump in the phase curve corresponding to the displacement of the average position of the shock. /19-5

3. Comparisons between Experimental and Computed Results

3.1 Presentation of Methods of Computation

Each of the methods of computation used will be briefly

presented. For more detail, refer to the works quoted as references.

a) Methods Based on the Hypothesis of Potential Flows

Steady Flows

The programs which are available use the GARABEDIAN and KORN methods to forecast steady flows in inviscid fluid in supercritical regime. The effects of viscosity are taken into account by pairing with a boundary layer calculation, with pairing technique consisting of computing the inviscid flow around the airfoil, enlarged by the thickness of displacement of the boundary layer (2.3).

Unsteady Flows in Inviscid Fluids, Subcritical Regime:

To deal with unsteady flows in the entire subcritical area , we can use the linear plane plate theory. This method, currently used in structural calculations by ONERA, is a doublet method (4): the airfoil is assimilated into a line without thickness or curve and broken down into about twenty elements, each comprising a doublet of the acceleration potential of the forward 1/4. The conditions of tangency of the flow are applied to the rear 1/4 of each element. This method is, however, of limited use, as it does not take into account the influence of the average flow in the unsteady response, an influence which is significant in heavily loaded configurations.

To represent the influence of the average flow on the unsteady response at low speeds, we have at our disposal a program for computing incompressible unsteady flow, developed by the Bertin company (5) and based on the GEISING method (6). The airfoil is represented by surfaces and recesses along its contours and eddies on the median line. The wake is composed of free eddies emitted at each time increment to preserve the total circulation of the flow. This method takes into account the exact form and movement of the airfoil, as well as the deformation of the eddying wake.

Unsteady Flow in Inviscid Fluid, Supercritical Regime:

In order to deal with unsteady flows in superc ritical regime, we currently use a computation program solving, by a method of finite differences, the equation for speed potentials with the appsoximation of small disturbances for transonic, two-dimensional unsteady flow. This program, initially developed for the study of flow over helicopter blades by F.X. Caradonna (7), was adapted to suit oscillating flaps by J.J. THIBERT of ONERA. There is also another method for small transonic disturbances being developed by the Structural Resistance department of ONERA (8) and which has the advantage of requiring a shorter computation time than does the CARADONNA program.

b) Solution of Euler Equations

The hypothesis of small disturbances is not very realistic for a 16% airfoil comprising supersonic zones, sometimes extensive, for an upstream infinite Mach number of the order of 0.73 to 0.75, and it is quite difficult to know what terms can be ignored in the potential equations.

To evaluate error due to the small transonic disturbances hypothesis, we will refer to a method for computing steady flow in inviscid fluids solving the Euler equations (9). This method makes it possible to compute, for an airfoil of a given thickness, supercritical flows, without restrictions on the intensity and movement of shocks. The inviscid flow around an airfoil with an oscillating flap is calculated by solving the complete Euler equations, in the form of integral laws of conservation, by the "finite volumes" method generalized as a mobile lattice. The method is conservative, in the sense that in a numerical evaluation of mass or quantity of movement or of energy in a field made up of cells, the contributions of the internal flows intervening in the numerical diagram cancel each other out in pairs. The condition of sideslipping is imposed on the oscillating flap in its exact position over time.

The main disadvantage of this last method, which is of

the type which is explicit in its present form, is the length of time required for computation.

This method was tested and perfected by a NACA 0012 airfoil with oscillating flap (9), but it was only possible to carry out two steady flow calculations with the RA 16 SC1 airfoil in time to include them in this article. Unsteady flow calculations are in progress.

c) Taking into Account Unsteady Viscous Effects

In order to take into account unsteady viscous effects, we carried out a pairing of a method of computation for inviscid fluids with a program for computation of unsteady turbulent boundary layer, simultaneously with incompressible flow, using the BERTIN program, and transonic flow, with the CARADONNA program.

All the results presented in this report were obtained with an integral method for calculating the turbulent boundary layer in unsteady compressible flow, developed at CERT (10). This method uses the Karman equation (conservation of quantities of motion) and the equation of entrainment established for unsteady flow, the added relationships required to solve the system of equations being the same as those used for steady flow.

Whether for incompressible or transonic flow, the method of pairing consists of making the inviscid fluid calculation with a modification of the limiting conditions on the airfoil to take into account the development of the boundary layer. In concrete terms, this means a flow of fluid across the wall characterized by normal speed v_e in the BERTIN program, and by a modification of the local slopes of the airfoil of quantity $(v/u)_p$ in the CARADONNA program. v_e and $(v/u)_p$ are given by the relationship:

$$\frac{v_e}{u_e} = \left(\frac{v}{u}\right)_p = \frac{1}{\rho_e u_e} \frac{\partial}{\partial x} \left(\rho_e u_e \delta_1\right)$$

where δ_1 is the thickness of displacement, u_e the tangential speed of inviscid flow and ρ_e the voluminal mass. /19-6

This relationship is dentical to that given by J.C. LEBALLEUR for steady flows (11): in fact, the pairing relationship at the wall causes

$$\frac{1}{\rho_e u_e} \int_0^\infty \left[\left(\frac{\partial \rho}{\partial t}\right)_\delta - \left(\frac{\partial \rho}{\partial t}\right)_y\right] dy$$

to appear as the single unsteady term which has been ignored even in compressible flow.

For each time interval, two or three iterations for inviscid fluid-boundary layer are carried out, with, if necessary, the use of a relaxation method.

The main problems encountered in pairing are essentially linked to the appearance of breakaway at the trailing edge, at the hinge and in the presence of shocks of significant intensity. The shock wave-boundary layer interactions and breakaway are treated in a simplified manner, and it is obvious that the pairing technique is only usable in the case of weak shock wave-boundary layer interaction and small breakaway zones.

3.2 Comparisons in Steady Flow

Figures 10 and 11 correspond to two control surface angles. For each angle, steady pressures measured with a guided jet were brought to $M_\infty = 7.3$ and calculations carried out for inviscid fluids with the potential method and with the Euler equations. These computations were carried out with the Mach number and incidence corrected for wall interference these correctionsbeing quite well known for guided jets. The two methods of calculation give fairly similar results, with a shock much farther downstream than in the experimental results, for the extrados. The shock calculated using the Euler equations is always

a little farther downstream than that computed using the potential method.

From the results presented in Figures 10 and 11, we drew experimental and theoretical quasi-steady values for the unsteady pressure coefficients; these values correspond to oscillation of the control surface at zero frequency with an amplitude of $\pm$ 0.59° around the average angle $\delta m = -1.07°$ (Figure 12). They are obtained as follows:

$$C_{Pqs} = \frac{K_p(\delta_1) - K_p(\delta_2)}{(\delta_1 - \delta_2)\,rad.} = \frac{K_p(-0{,}48°) - K_p(-1{,}66°)}{1{,}18 \cdot \pi / 180}$$

The peak due to the displacement of the shock is still much farther downstream in invised fluid theories than in the experiment, the one given by the Euler equations being slightly farther downstream than that given by the potential theory. The two theories given very similar results upstream from the shock, but, on the other hand, they differ sharply downstream from the shock and on the flap.

In figures 13 to 15, which correspond to three control surface angles, the experimental steady pressures are presented along with those calculated using the potential theory with and without boundary layer (2,3).

The agreement between the experiment and the theory with /19-8
boundary layer is relatively good, except, perhaps, immediately downstream from the shock, where the theory often indicates a reacceleration which is not found experimentally, and on the extrados of the flap, where computations diverge notably from the experimental results.

To explain these discrepancies, it must be noted that the shock wave boundary layer interaction is treated in a simplified manner

in the computation, and that there may exist a draft effect through the slit between the wing and the control surface which cannot be taken into account in computation. In addition, in the three selected configurations, computations did not always converge very successfully and almost always indicated breakaway on the control surface, which limits the validity of the results.

We also compared the experimental quasi-steady values with the values given by the potential flow theory, with and without boundary layer (Figure 16) in the same situation as in Figure 12.

We noted a certain dispersal of experimental quasi-stationary values for the intrados, as they are obtained by differences in Kp which have very similar values.

Figure 16 shows the advantage of the computation with boundary layer, in particular in order to position the shock displacement peak correctly. But the part downstream from the extrados shock, espeically on the flap, is still rather poorly predicted by the theory using the boundary layer. It is therefore most important to improve the treatment of the shock wave - boundary layer interaction, and of breakaway.

3.3 Comparisons in Unsteady Flow

3.3.1 Subcritical Zone

At low Mach numbers, the linearization theory predicts the development of unsteady pressures along the chord with fair success (figure 17), but it does not differentiate between the extrados and the intrados because it does not take into account the effects of the average flow on the unsteady flow, so that its use is limited to lightly loaded configurations. In this case, it benefits from a fortunate compensation between the effects of thickness and curvature on one hand and viscosity on the other, effects which are already acting in

the opposite direction in quasi-steady mode (12). /19-9

It will be noticed that this linear theory gives infinite unsteady pressures at the leading edge and at the hinge.

In Figure 18, one of the experimental cases presented with the linear theory in Figure 17 is compared with the results of the Bertin company's program for inviscid flow computation with and without pairing with a computation for unsteady turbulent boundary layer. The inviscid flow computation program gives stronger moduli of unsteady pressure than does the linear theory, (see Figure 17), but it differentiates well between the intrados and the extrados and gives a better qualitative representation of the unsteady phenomenon, especially in the vicinity of the leading edge and of the hinge. The gain obtained by pairing it with the boundary layer computation is appreciable: the discrepancy in the unsteady pressure moduli between the inviscid flow computations and the experimental results is reduced by more than 50%.

The phases are almost unchanged by this pairing, except in the vicinity of the trailing edge.

The advantage of pairing appears even more strongly in Figure 19 which represents a case of strong viscous interaction, with an average flap angle of 5°: when the flap is angled 5° in steady flow, a breakaway occurs at the extrados trailing edge, in the neighborhood of $x/c = 0.95$. Calculations for unsteady inviscid flow provide very different results from those obtained experimentally. Pairing with boundary layer computations reduces, by nearly 70%, the discrepancy between the unsteady pressure moduli and causes the phases to evolve in a forward direction. The paired computation fairly well represents the evolution of unsteady pressures along the chord up to about $x/c = 0.9$: on the extrados a very pronounced phase advance behind the hinge, and an increase in the moduli of unsteady pressures towards the trailing edge, can be observed. However, the last ten per cent of

the chord is unrealistic because of the simplified treatment of the breakaway zone. This results in a lack of exactitude in the quantitative values of the moduli and phases of unsteady pressures on the airfoil as a whole. The paired program is thus functioning here at the limit of its potential.

If we consider the intensity of the unsteady pressures between the leading edge and the hinge, for example, (Figures 17 and 18), non-linear computation paired with the boundary layer may appear /19-10
disappointing in comparison to the linearized theory which gives a roughly equivalent result, since it benefits from an error compensation between the effects of thickness and curve on one hand, and viscous effects on the other.

However, by suppressing the infinite values of the leading edge and the hinge, by giving much better results than those of the linearized theory for the flap, and by being very sensitive to the average flow parameters, paired non linear computations give results which are much more satisfactory from the point of view of overall coefficients. This is shown in Figures 20 to 22:

- Figure 20 first shows the evolution of the three unsteady coefficients (lift, moment of pitch at 25% and moment of hinge) as a function of the reduced frequency at $M_\infty = 0.3$ in configurations in which the average angle of the control surface is nil. The experimental results are presented with those of the linear theory and of the BERTIN program with and without boundary layer. The paired program gives better results than the linear theory, but it does not give satisfactory results for the phase of the moment of hinge. It should however be noted that the experimental determination of the unsteady moment of hinge lacks precision as a result of the limited number of pressure gauges on the flap (10 in all), the one farthest downstream being located only at $x/c = 0.95$. In addition, there may be a draft between the wing and the control surface which the theory does not take into consideration.

- the advantage of using the paired program is still more apparent in Figure 21, which shows the evolution of the same three overall unsteady coefficients as a function of the average angle of the control surface for a given reduced frequency at $M_\infty = 0.3$. The coefficients given by the linear theory are constant, since according to the hypothesis the unsteady flow does not depend on the average flow. The coefficients given by the BERTIN program for inviscid fluids vary very slightly when the average angle of the control surface varies between -10° and $+10^\circ$. On the other hand the unsteady coefficients of lift and moment of pitch given by the paired program are quite close to the experimental coefficients and evolve in the same way with the average angle: the modulus decreases more and more quickly as the average load on the wing increases and the phase evolves in a forward direction as we approach configurations in which breakaway occurs. It will be noted, moreover, that the paired computation does not give phases which are different from those of the inviscid flow computations except on approaching breakaway configurations, in the vicinity of $\delta_m = 5^\circ$. The paired computation was not pursued beyond $\delta_m = 5$ because of the large extent of the breakaway zones. We may therefore conclude that the phenomenon of dependency on the average angle which affects the unsteady performance of the control surfaces is essentially of viscous origin.

As far as the moment of hinge is concerned, the paired computation shows evolution as a function of the average angle to be more significant than does the inviscid flow computation, but the theoretical values differ increasingly from the experimental values for large angles, which can be explained by the reasons already given.

Apart from this lack of precision on the moment of hinge, the paried program thus offers a number of advantages, from the point of view both of predicting unsteady coefficients, and of predicting average values, as shown in Figure 22 where the average values of the lift coefficient as a function of the average angle of the control surface are shown.

In order to attempt an explanation of the discrepancies noted between the experimental results and those of the paired program, it should be remembered that the boundary layer was presumed to be entirely turbulent from a point arbitrarily located about 8% from the leading edge. In addition, the test results have not been corrected for the wall interference.

3.3.2 High Subsonic and Supercritical Zone

The linear theory being incapable of anticipating the existence of shocks, only comparisons with the CARADONNA program for small transonic disturbances will be considered.

In supercritical regime, the position of the shocks is a crucial point, and is strongly influenced by the wall This is why the computations were carried out at an incidence and Mach number corrected for the steady wall effect, the only one which can presently be estimated with validity. In guided jet, this wall effect can be assimilated with a Mach number correction and could be estimated correctly as can be seen in the steady computations (Figures 13 to 16). In permeable jet, the wall effect was estimated empirically and assimilated with a correction of incidence proportional to the average lift coefficient for a given Mach number.

In any case the variations in lift due to small movements of the control surface (1° of amplitude) being relatively small, we suppose, a priori, that the purely unsteady wall effects have a limited influence on the results, even for already significant reduced frequencies of the order of 0.165 or 0.235.

Figure 23 shows the distribution of local unsteady lift, $\Delta C_p = C_{p\,INTR.} - C_{p\,EXTR.}$, along the chord, in modulus and phase, in permeable jet at $M_\infty = 0.6$, a Mach number above which the first sonic points begin to appear on the extrados leading edge in steady flow. /19-12
In this case, the small transonic disturbances method, paired with

computation of the boundary layer, give very good results, the effect of the pairing being to diminish the moduli (as in low subsonic) but to accentuate the phase delay, for a moderately loaded configuration (C_z average ≈ 0.3).

Figures 24 and 25 present the evolutions along the chord of the extrados unsteady pressures at two other Mach numbers for which a shock is observed at the same reduced frequency and in the same jet configuration as at $M_\infty = 0.6$. Figure 26 shows an example in guided jet.

Overall, inviscid flow calculations by the method of small transonic disturbances predict fairly well the appearance of experimental phenomena with peaks on the curve of the moduli and more or less accentuated phase leaps linked to the displacement of the shock. These singularities are located farther downstream than in the experiments, but they are much better placed and the order of size of the unsteady pressure moduli is more correct when the boundary layer is taken into account.

However, when the shock occurs at less than 30% from the leading edge, either by inviscid flow computations (Figure 24) or because of the boundary layer (Figures 24 and 25) it loses its character of singularity and gives rise to an insignificant maximum on the moduli. This is perhaps attributable to the fact that the method of small disturbances lacks precision at the leading edge, especially for a 16% airfoil.

For the guided jet example (Figure 26) at an already /19-13
large Mach number and reduced frequency, even though the Mach number correction was satisfactorily estimated according to calculations carried out for steady flow (Figures 13 to 16), the present paired computations bring the shock forward a little too much, while the order of size of the unsteady pressures remains correct. Where the phase is concerned, as the inviscid flow, in this case, already gives

insufficient delay at the leading edge, the boundary layer accentuates this descrepancy by reducing the size of the supersonic zone, the source of the delay. Upstream from the shock, the boundary layer acts as it does at $M\infty = 0.6$, bringing about a fairly significant phase delay.

Figure 27 summarizes, for several examples, the average value, the amplitude of variation and the phase of lift, both experimental and theoretical, with and without boundary layer.

4. Conclusion

This study shows that in many cases, the unsteady aerodynamic response due to a movement of the control surface depends to a large degree on the conditions of the average flow over the airfoil and control surface as a unit. It seems that this phenomenon is due largely to viscosity. The use of linear theories to preduct unsteady aerodynamic responses is therefore in fact very limited, and it is necessary to have recourse to non-linear inviscid flow methods which should be paired with a boundary layer calculation.

In this respect the results of the first attempts at pairing are encouraging. However, it is necessary to have the inviscid flow method which is as exact as possible, without forgetting the compromise between the desired precision and speed of calculation. In addition progress remains to be made in pairing techniques, espeically where the treatment of breakaway zones and shock wave-boundary layer interactions are concerned. Finally, an effort should be made to take into account, either experimentally or by calculation, the unsteady boundary effects.

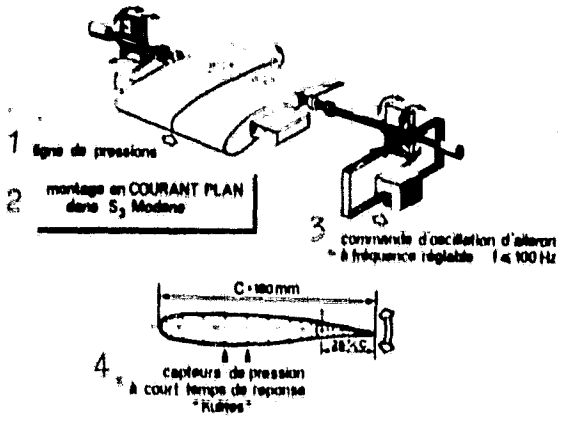

Key: 1. Pressure line
2. PLANE CURRENT assembly in Modane S3
3. Adjustable-frequency aileron oscillation control f $\leq$ 100 Hz
4. Short-response-time "Kulite" pressure gauges

Figure 1: Assembly with oscillating aileron on a thick supercritical airfoil

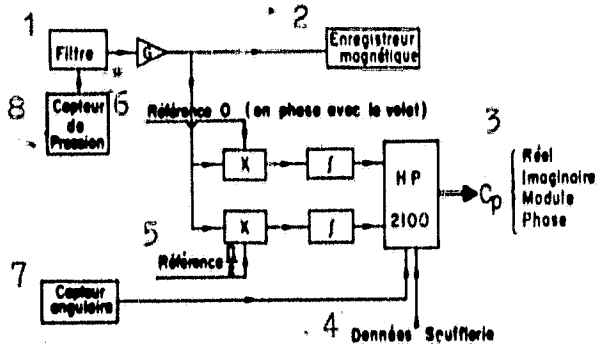

Key:
1. Filter
2. Magnetic recorder
3. Real, Imaginary, Modulus, Phase
4. Data Wind Tunnel
5. Reference $\frac{\Pi}{2}$
6. Reference 0 (in phase with flap)
7. Angle gauge
8. Pressure gauge

Figure 2: System of unsteady measurements

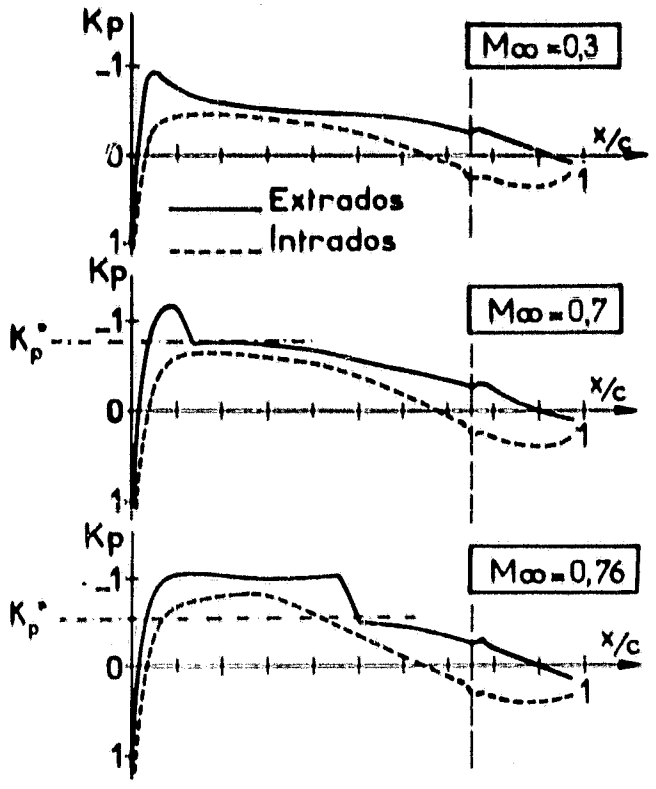

Figure 3: SNIAS airfoil 16SC1 - $\alpha = 0^\circ$; $\delta = 0^\circ$ = distribution of pressure in steady flow

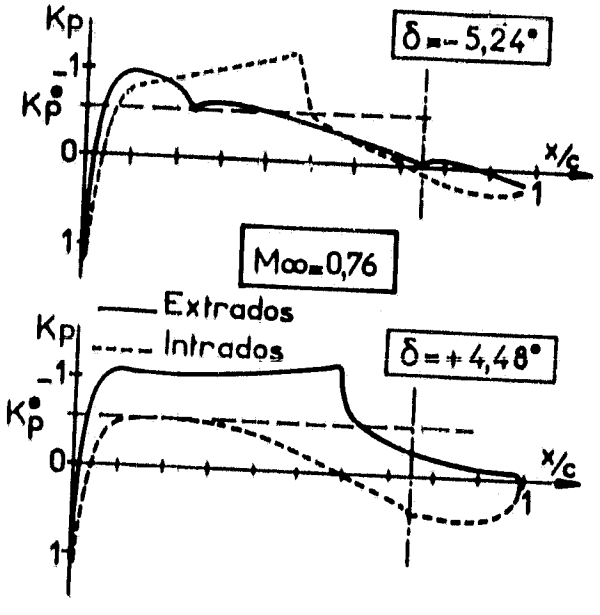

Figure 4: Efficiency of the control surface in steady flow. $\alpha = 0^{\circ}$

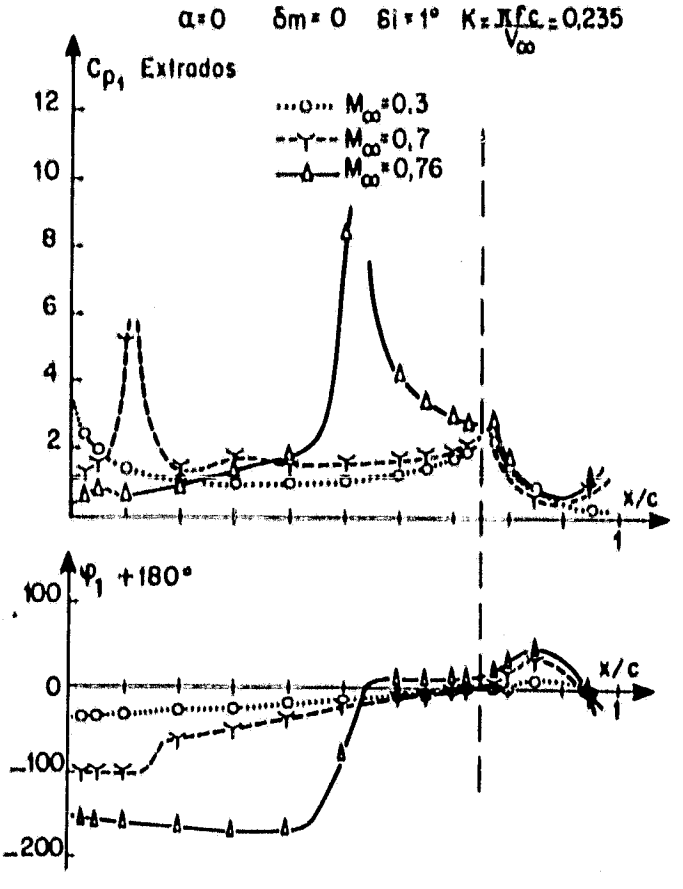

Figure 5: Influence of the Mach number on unsteady pressures

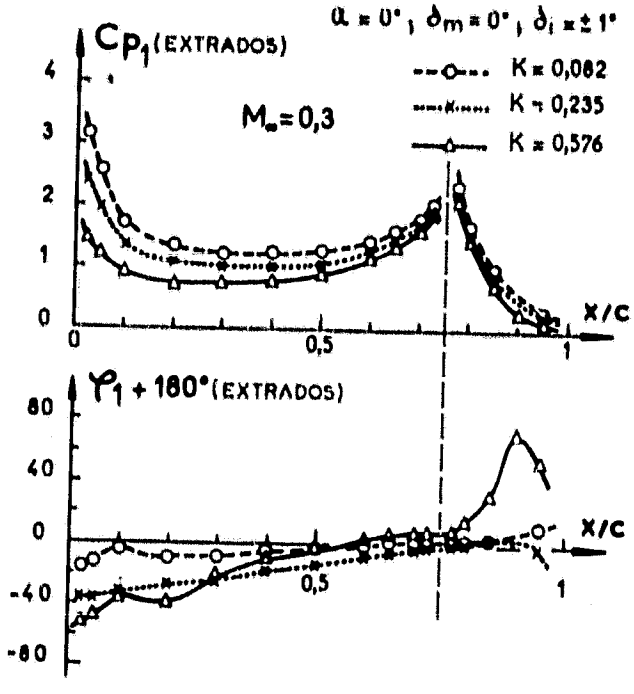

Figure 6: Influence of reduced frequency on unsteady pressures

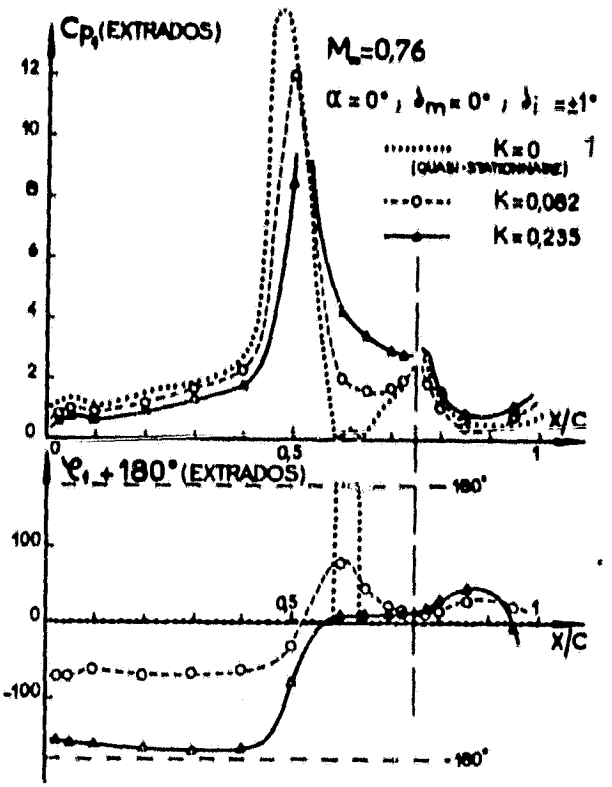

Figure 7: Influence of the reduced frequency on unsteady pressures

Key: 1. Quasi-steady

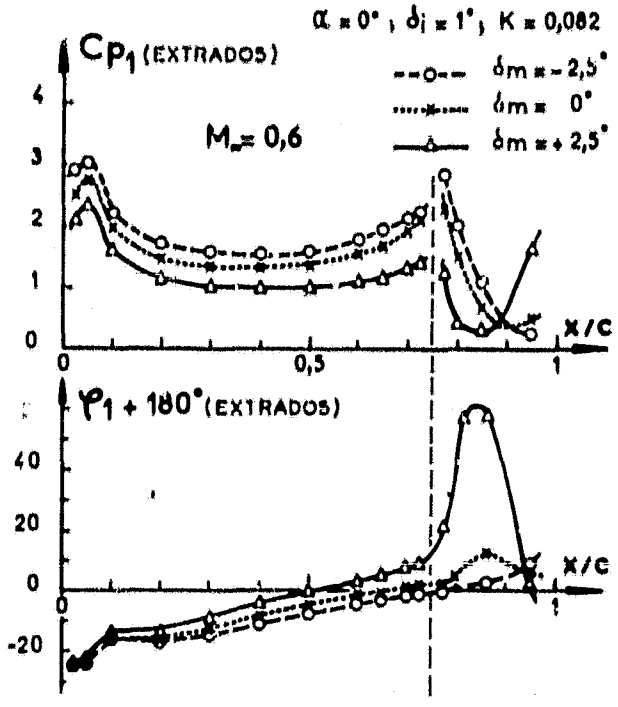

Figure 8: Influence of average angle δ_M on unsteady pressures

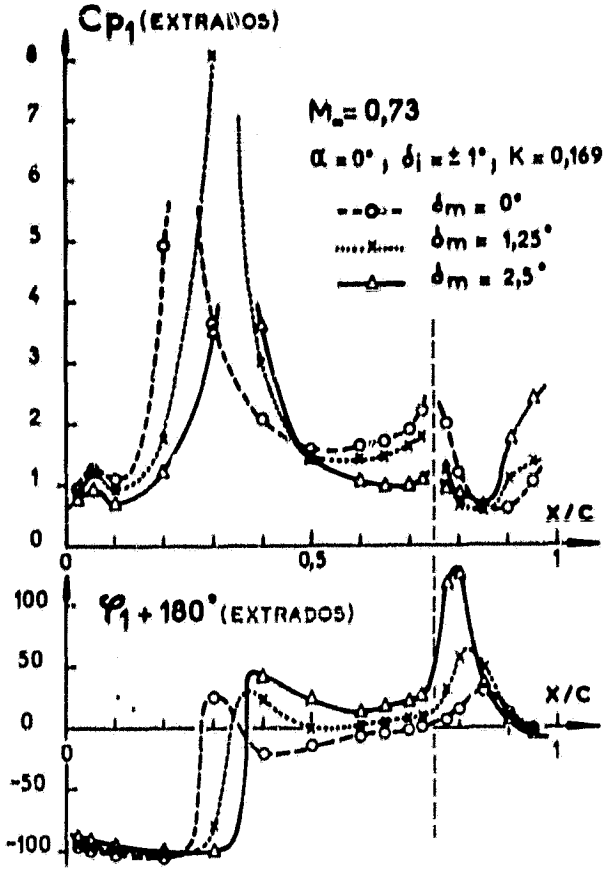

Figure 9: Influence of average angle δ_m on unsteady pressure

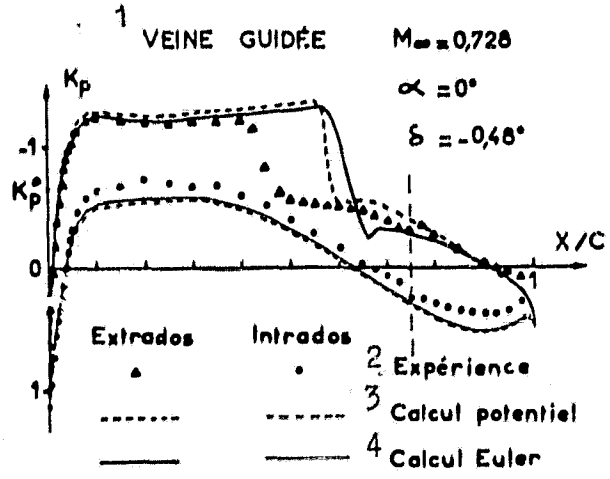

Figure 10: Comparison between calculation and experimental values in steady transonic flow.

Key: 1. Guided jet
2. Experiment
3. Potential calculation
4. Euler calculation

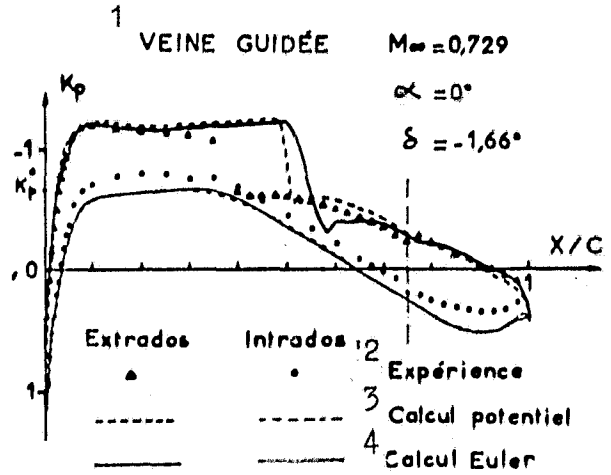

Figure 11: Comparison between calculation and experimental results in steady transonic flow.

Key: 1. Guided jet
2. Experiment
3. Potential calculation
4. Euler calculation

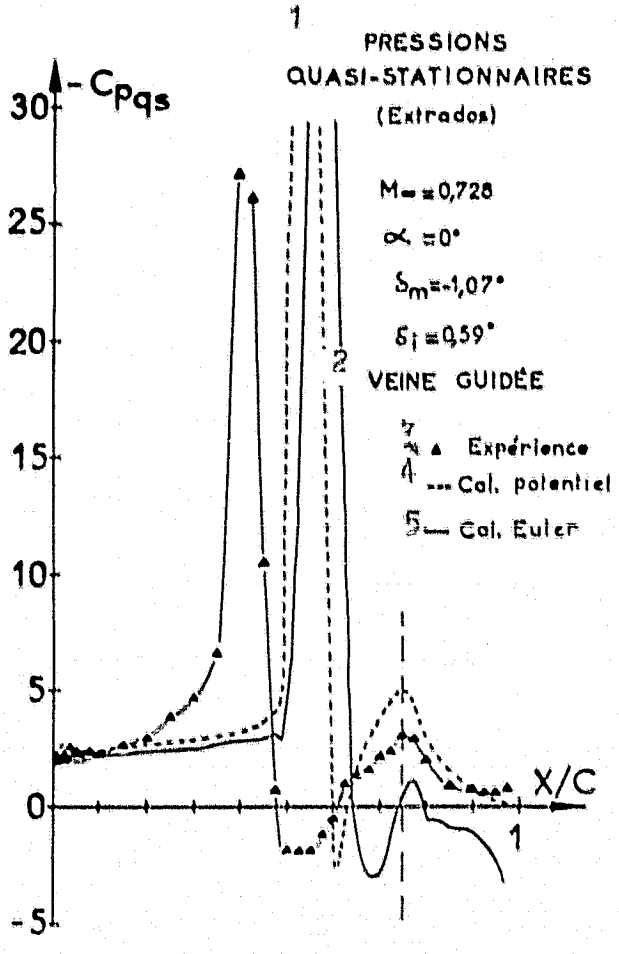

Key: 1. Quasi-steady pressures (extrados)
2. Guided jet
3. Experiment
4. Potential flow calculation
5. Euler Calculation

Figure 12: Comparison of calculated and experimental results for quasi-steady and transonic values

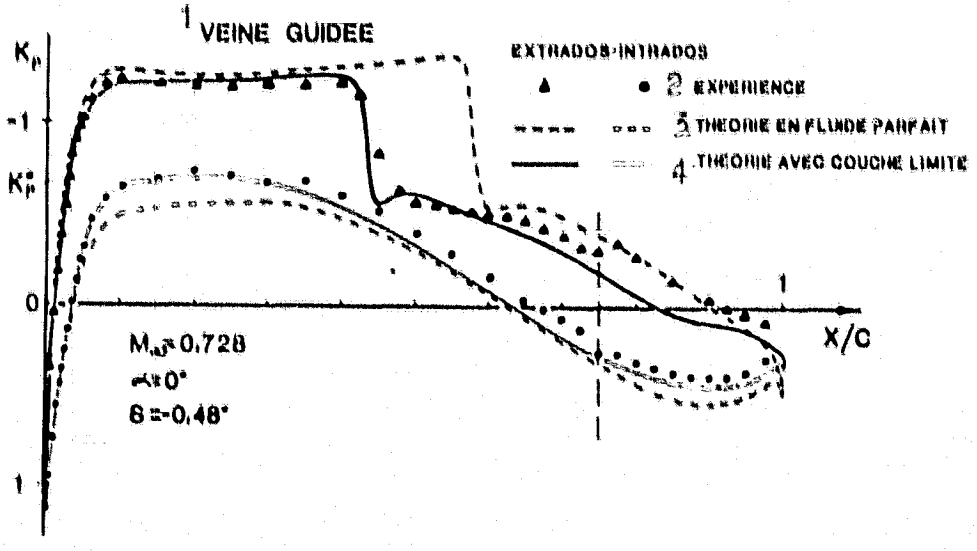

Key: 1. Guided jet
2. Experiment
3. Inviscid flow theory
4. Boundary layer theory

Figure 13: Comparison of calculated and experimental results for steady transonic flow

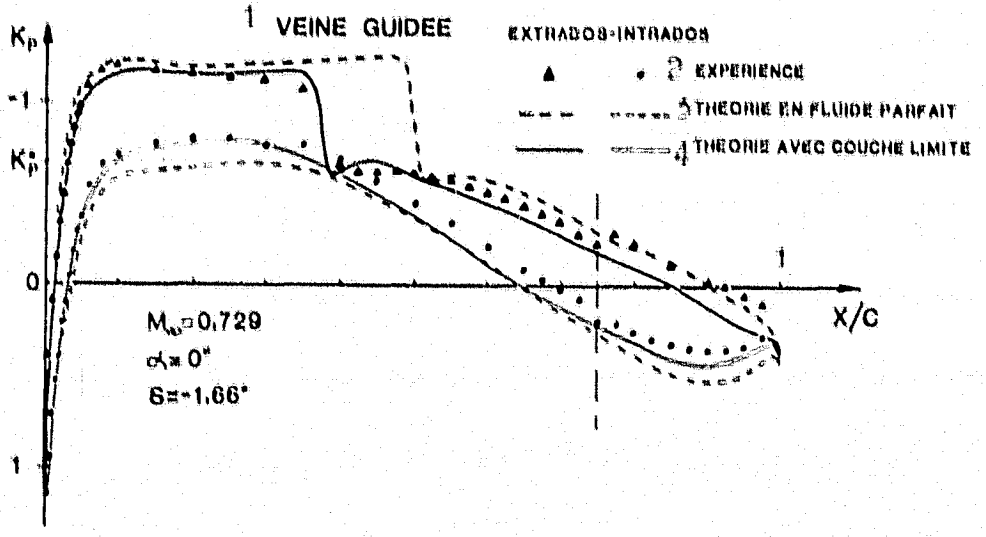

Key: 1. Guided jet
2. Experiment
3. Inviscid flow theory
4. Boundary layer theory

Figure 14: Comparison of calculated and experimental results for steady transonic flow

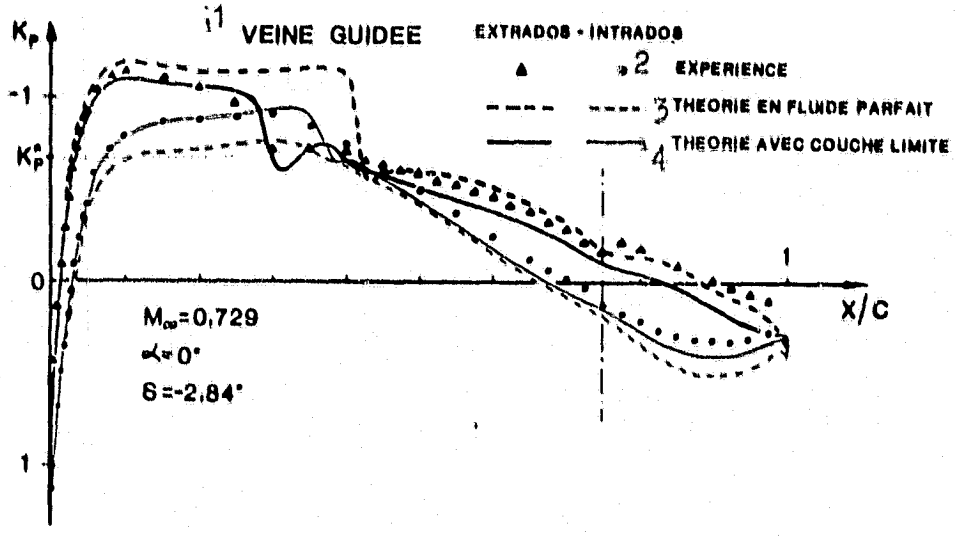

Key: 1. Guided jet
2. Experiment
3. Inviscid flow theory
4. Boundary layer theory

Figure 15: Comparison of calculated and experimental results for steady transonic flow

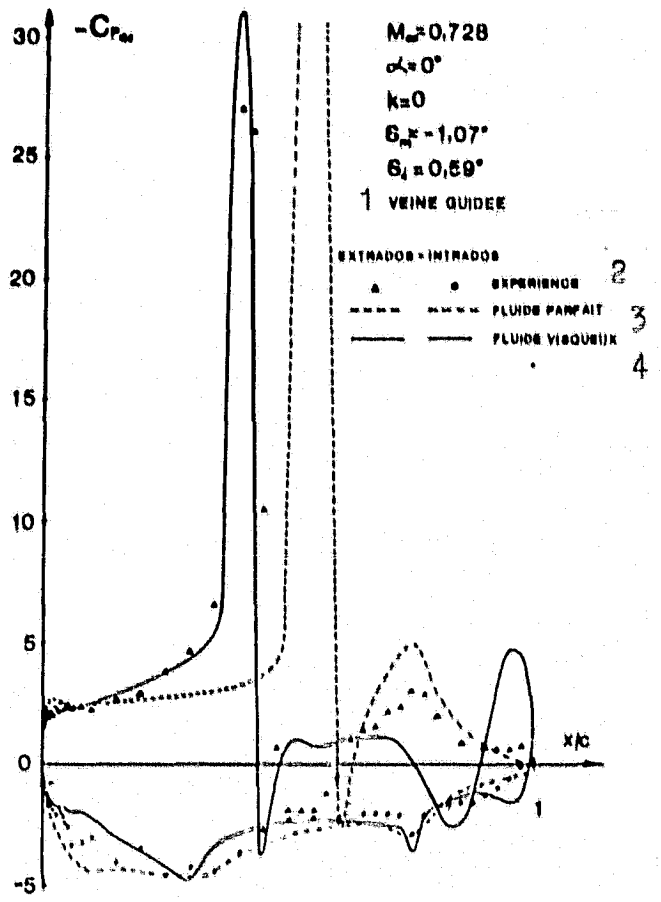

Key: 1. Guided Jet
2. Experiment
3. Inviscid flow
4. Viscous flow

Figure 16: Comparison of experimental and calculated quasi-steady values in transonic flow.

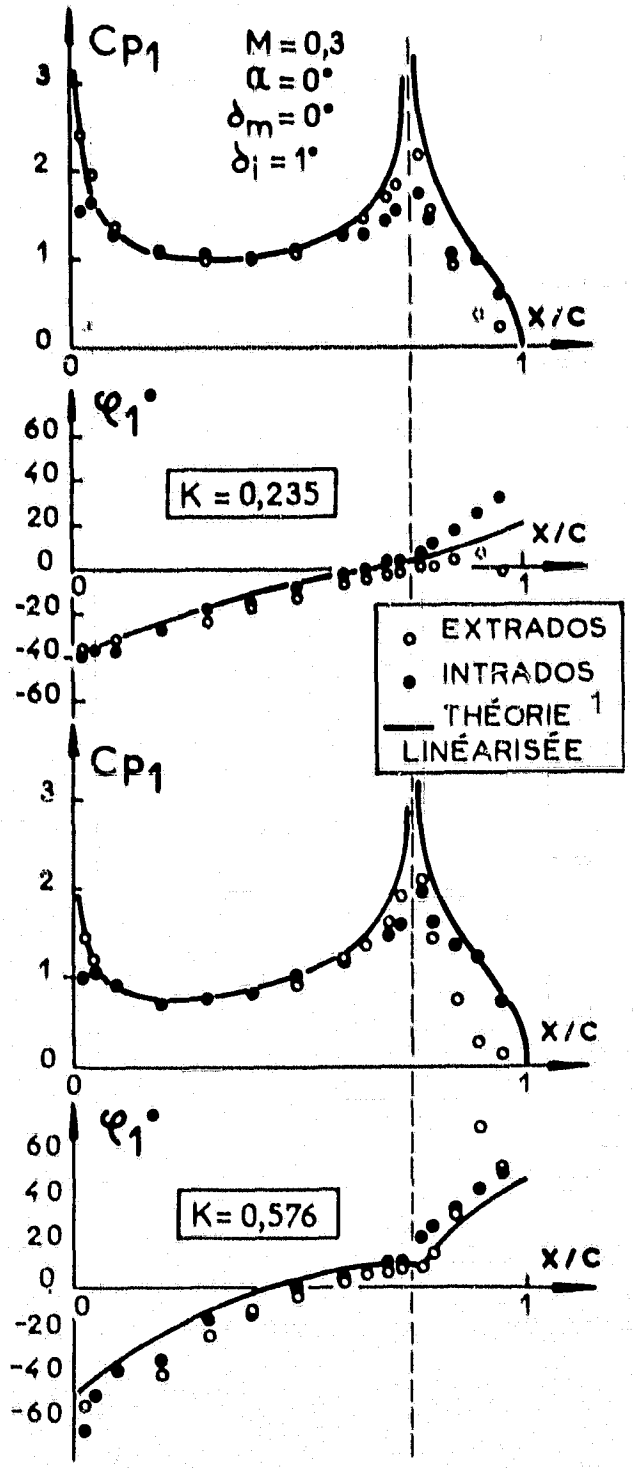

Key: 1. Linear theory

Figure 17: Comparison of experimental unsteady pressures with the subsonic linear theory.

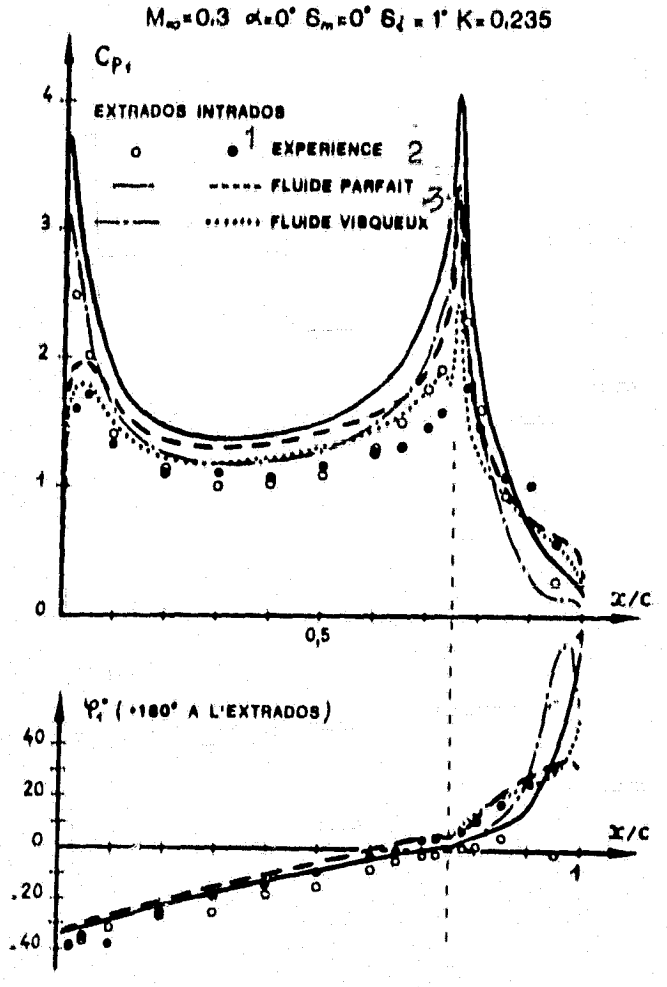

Key: 1. Experiment
2. Inviscid flow
3. Viscous flow
4. +180° to extrados

Figure 18: Comparison of calculated and experimental values: demonstration of the effects of viscosity in unsteady flow.

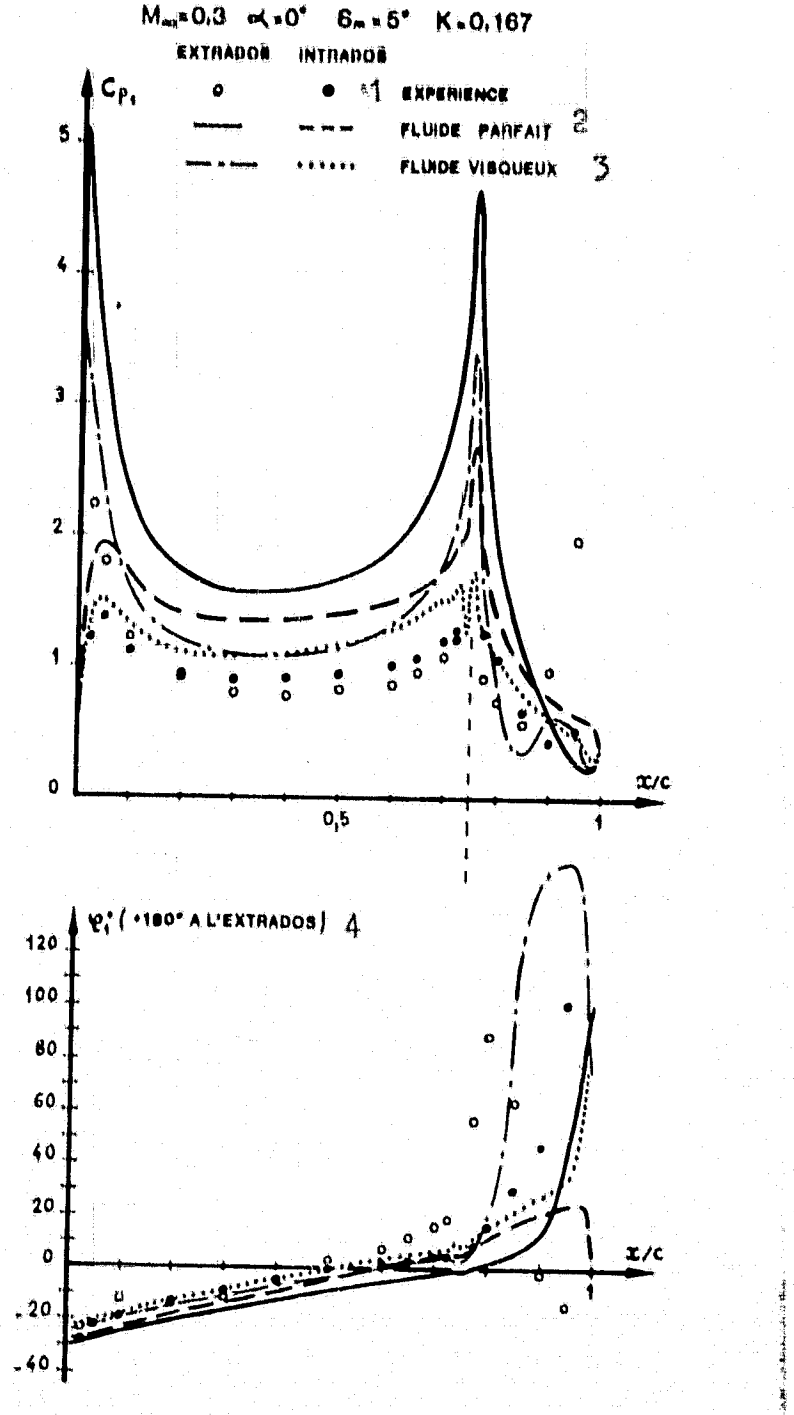

Key: 1. Experiment
2. Inviscid flow
3. Viscous flow
4. +180° to extrados

Figure 19: Comparison of calculated and experimental values: Demonstration of the effects of viscosity in unsteady flow.

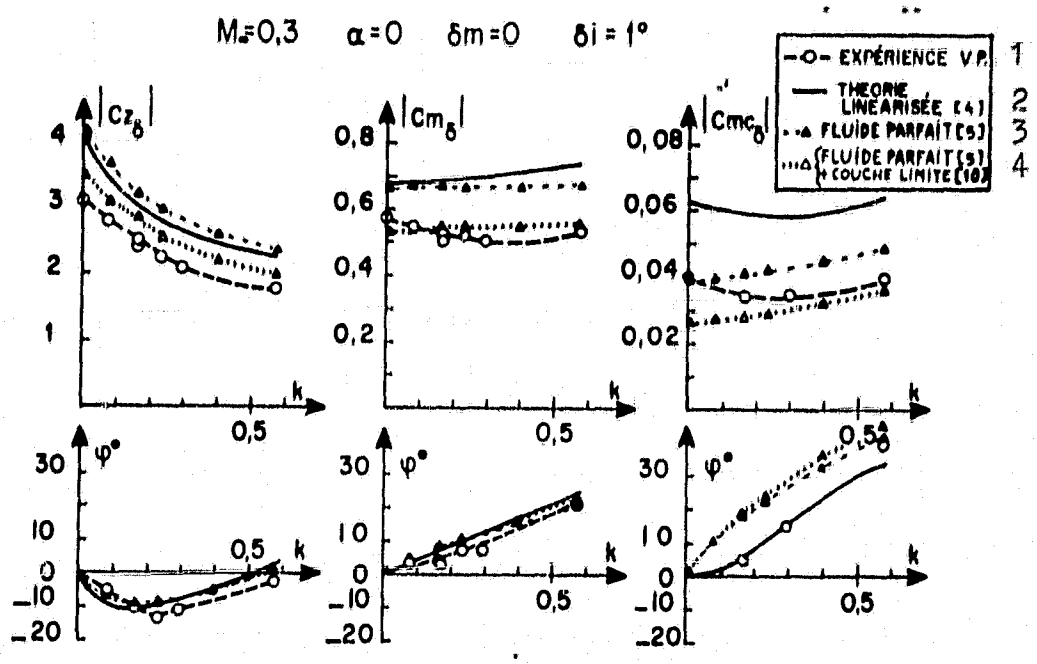

Key: 1. Experiment, permeable jet 3. Inviscid flow
2. Linear theory 4. Inviscid flow + boundary layer

Figure 20: Unsteady coefficients of lift, moment of pitch and moment of hinge: influence of reduced frequency, comparison of calculated and experimental values

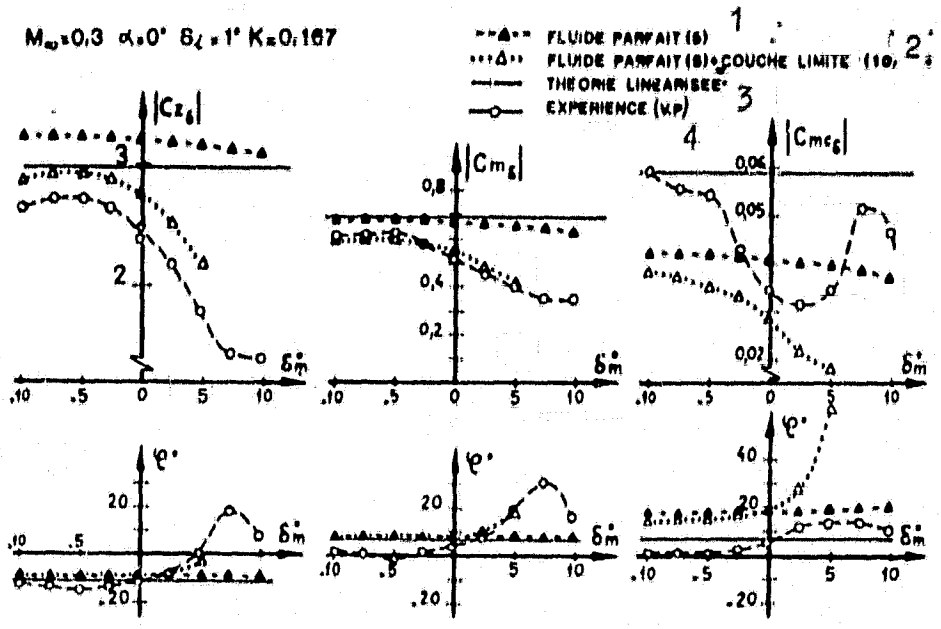

Key: 1. Inviscid flow
2. Inviscid flow + boundary layer
3. Linear theory
4. Experiment (permeable jet)

Figure 21: Unsteady coefficients of lift, moment of pitch and moment of hinge: influence of average angle

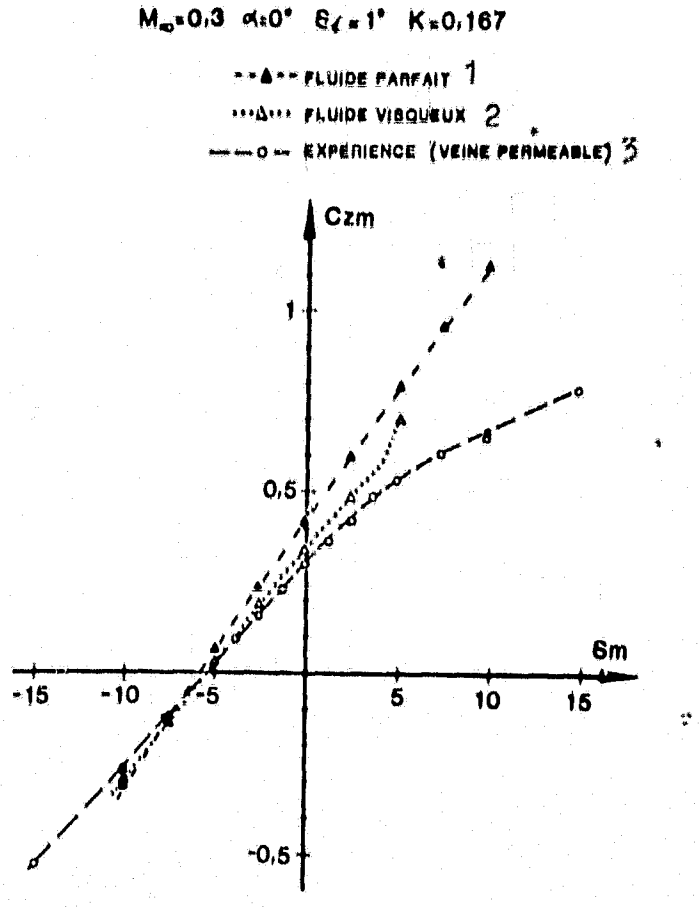

Key: 1. Inviscid flow
2. Viscous flow
3. Experiment (permeable jet)

Figure 22: Comparison of calculated and experimental average lift values.

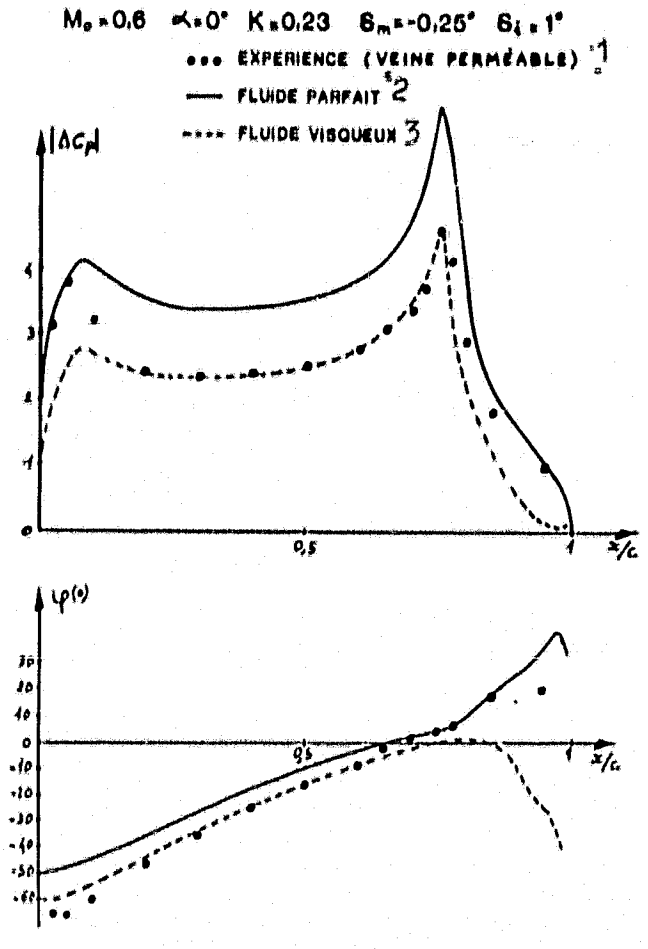

Key: 1. Experiment (permeable jet)
2. Inviscid flow
3. Viscous flow

Figure 23: Comparison of experimental unsteady pressures with the theory of small transonic disturbances and demonstration of viscous effects

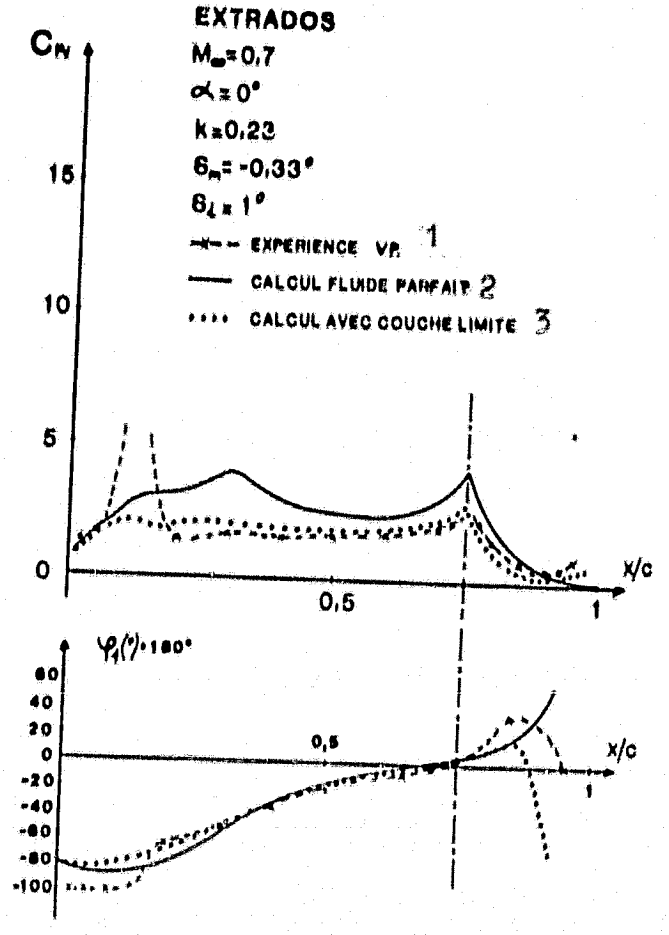

Key: 1. Experiment, permeable jet
2. Calculation with inviscid flow
3. Calculation with boundary layer

Figure 24: Comparison of experimental unsteady pressures with the theory small transonic disturbances and demonstration of viscous effects.

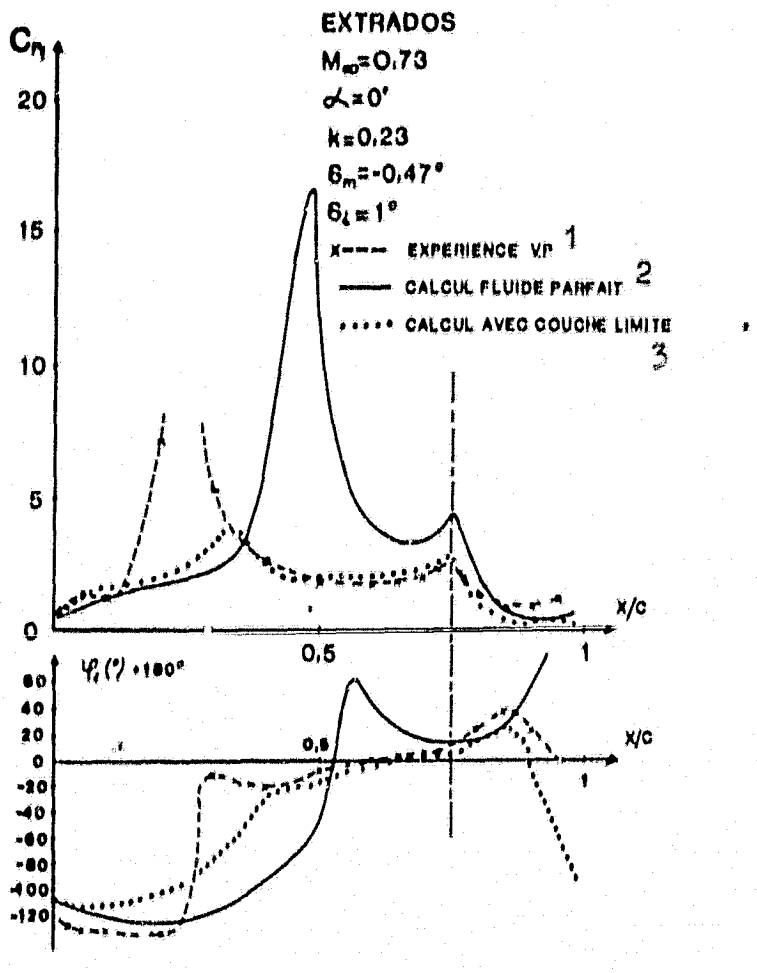

Key: 1. Experiment, permeable jet
2. Calculation with inviscid flow
3. Calculation with boundary layer

Figure 25: Comparison of experimental unsteady pressures with the theory of transonic small disturbances and demonstration of viscous effects.

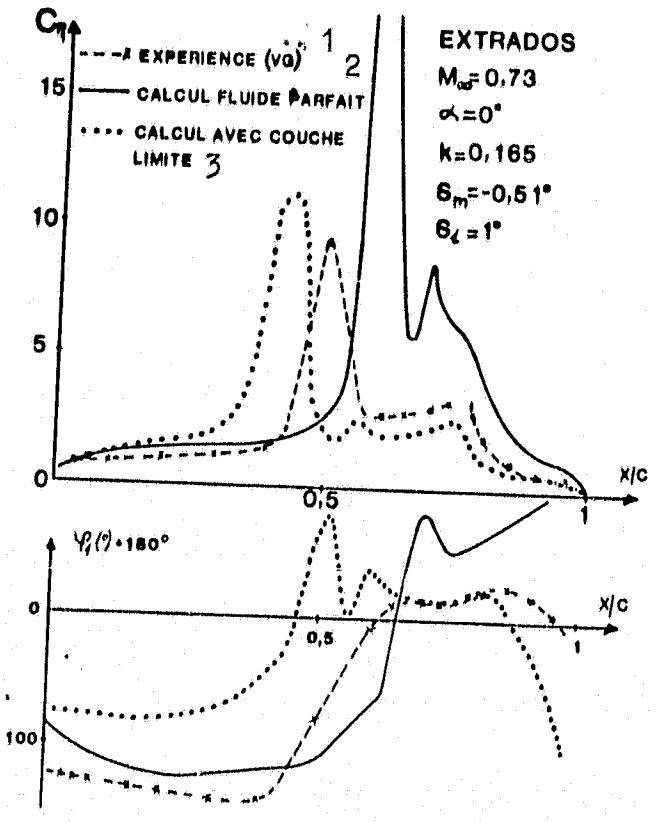

Key: 1. Experiment (guided jet)
2. Calculations with inviscid flow
3. Calculations with boundary layer

Figure 26: Comparison of experimental unsteady pressures with the theory of transonic small disturbances and demonstration of viscous effects

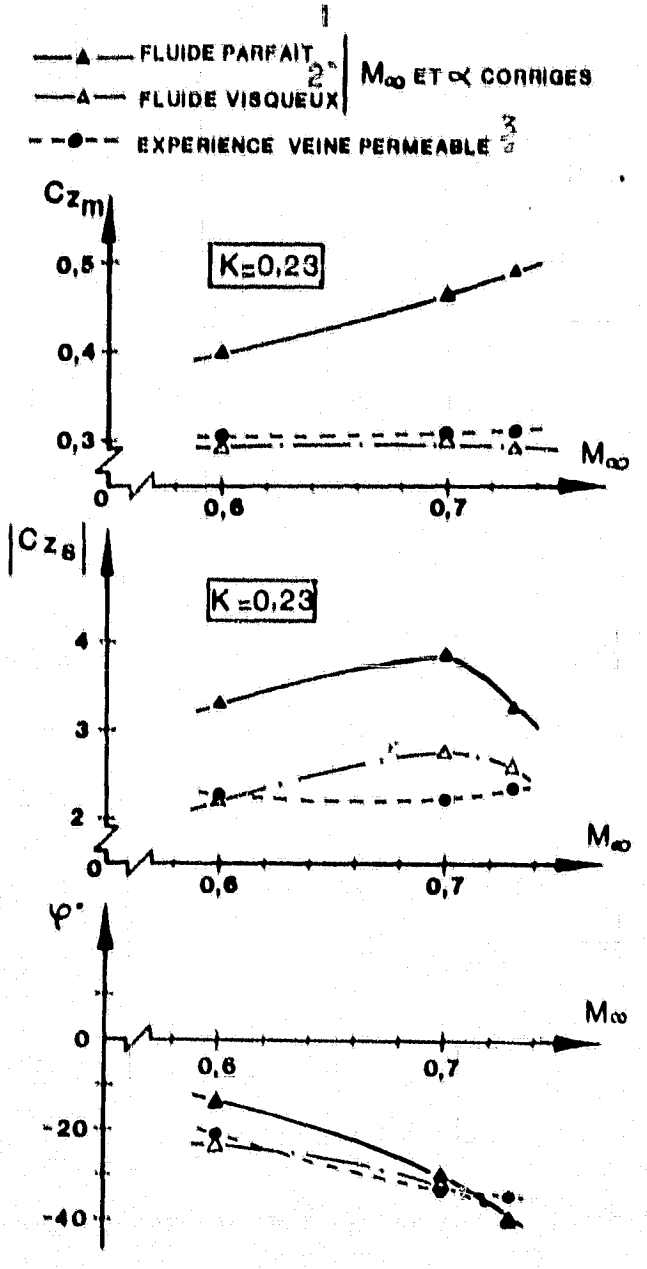

Key: 1. Inviscid flow
2. Viscous flow
3. M ∞ and α corrected
4. Experiment, guided jet

Figure 27: Comparison of calculated and theoretical results on the average value, amplitude of variation and phase of lift in transonic regime: demonstration of viscous effects.

REFERENCES

1. Grenon, R., and Thers, J., "Study of a supercritical airfoil with oscillating control surface in subsonic and transonic flow", AGARD CP 227.

2. Bavitz, "An analysis method for two-dimensional transonic viscous flow", NASA TN/D 7718.

3. Bousquet, J., "Two dimensional transonic calculations with boundary layer", 11th AAAF Conference, 1974.

4. Albano, E., and Rodden, W.P., "A doublet lattice method for calculating lift distributions on oscillating surfaces in subsonic flow", AIAA Journal, vol. 7, no. 2 (1969).

5. Baudu, N., and Le, Th., "Study of aerodynamic behavior of an airfoil with oscillating control surface", R.S.F. Bertin, Report 75 CC 06 (1075).

6. Giesing, J.P., "Non linear two dimensional Unsteady potential flow with lift", Journal of Aircraft, Vol. 5, no. 2 (1968).

7. Caradonna (F.X., (USA AMERDL), Philippe, J.J. (ONERA), "The flow over a helicopter blade tip in the transonic regime", ONERA TP 1976-115.

8. Couston, M., and Angelini, J.J., "Solution of Nonsteady two dimensional Transonic small disturbances Potential Flow Equation. ONERA T.P. 1978-68. Report presented at the Symposium on Unsteady Fluid Dynamics organized by ASME, San Francisco, December 10-15, 1978.

9. Lerat, A., Sides, J., "Numeric simulation of transonic flows using the integral form of the Euler equations", ONERA-T.P. 1979-10, Report presented at the 21st Annual Conference on Aviation and Astronautics, Tel Aviv and Haifa (Israel), Feb. 28 - March 1, 1979.

10. Cousteix, J., Houseville, R., Desopper, A., "Experimental results and methods of computation relating to turbulent boundary layers in unsteady flow", AGARD CP 227 (1977).

11. Le Balleur, J.C., "Viscous - Non-Viscous Pairing: analysis of the problem including breakaway and shock waves", La Recherche Aerospatiale 1977, no. 6 (November-December).

12. Tijdeman, H., and Destuynder, R., "Comments on transonic and Wing Store Unsteady aerodynamics: High subsonic and transonic effects in Unsteady aerodynamics, by H. Tijdeman", AGARD report 636.